ISSN 2070-0482, Mathematical Models and Computer Simulations, 2022, Vol. 14, No. 5, pp. 819–828. © Pleiades Publishing, Ltd., 2022.
Russian Text © The Author(s), 2022, published in Matematicheskoe Modelirovanie, 2022, Vol. 34, No. 3, pp. 101–116.

Atomistic Simulation of the Coexistence of Liquid–Vapor Phase States for Gold and Determination of Critical Parameters

V. I. Mazhukin[a], O. N. Koroleva[a, *], M. M. Demin[a], A. V. Shapranov[a], and A. A. Aleksashkina[a]

[a] *Keldysh Institute of Applied Mathematics of RAS, Moscow, Russia*

**e-mail: koroleva.on@mail.ru*

Received January 18, 2022; revised January 18, 2022; accepted February 21, 2022

Abstract—The work is devoted to the study (on the example of gold) of the properties of metals near the critical point. Long-term studies testify to the complexity of the problem and its importance both for constructing theoretical ideas about the behavior of metastable states of a highly superheated liquid phase of metals and for developing a number of technological applications in the field of materials science, the impact of concentrated energy flows on a substance, etc. Metastable states of a superheated liquid and a saturated vapor in the vicinity of the critical point have not been sufficiently studied. When approaching the critical point, the properties of matter change dramatically due to strong stochastic fluctuations of parameters (primarily density). Molecular dynamics (MD) methods are a relevant tool for determining critical parameters. For gold, they were used to obtain a liquid–vapor coexistence curve, from which the critical parameters were then determined: temperature, density, and pressure. In the calculations, the potential of the family of "embedded atom method" (EAM) was used as the interaction potential of particles. The value of the critical temperature T_{cr} was determined from the results of MD simulation using the method of the maximum size of the averaged cluster on the temperature curve passing through the critical region. The value of the critical pressure P_{cr} was obtained from the results of MD simulation from the temperature dependence of the saturated vapor pressure $P_{sat}(T)$. The value of the critical density ρ_{cr} was obtained from the results of MD simulation of the liquid–vapor coexistence curve using the empirical rule of the rectilinear diameter. The simulation results of this work are compared with the results of estimation of the critical parameters of gold by other authors using different approaches.

Keywords: molecular dynamics modeling, liquid–vapor coexistence curve, critical parameters, gold

DOI: 10.1134/S207004822205009X

1. INTRODUCTION

Determining the parameters of the critical points of the liquid–vapor phase transition in metals is important both from a theoretical and practical point of view. Of special importance are the critical parameters of transition metals, including gold, which are the most widely used for the development of promising structural materials and alloys [1]. However, the study of the thermodynamic properties of substances near their critical points is a difficult task. This is explained by many factors, including the variety of states of matter, characterized by a high energy density. Examples of such states are: hot compressed matter, strongly bound plasma, hot expanded liquid and quasi-ideal plasma. The knowledge of these conditions is limited. The complexity of physical processes causes difficulties in theoretical modeling, and the characteristics of these states at critical points are too high for accurate experimental measurements. Only the low-temperature branches of the binodal can be extracted from the measurements. In addition, when approaching the critical point, the properties of matter change, which is associated with the emergence of new phenomena and mechanisms of interaction between the particles of matter, such as fluctuations in the parameters of matter (primarily density), the values of which increase very rapidly when approaching the critical point. In such a situation, consideration of the critical state on the basis of a theoretical approach using thermodynamic functions is applicable only in the region where the fluctuations are relatively small [2].

Due to the complexity of conducting experiments at high temperatures, the critical point parameters were obtained only for a small number of substances, including alkali metals and mercury, which have relatively low temperature characteristics [3–6]. For most metals in static experiments, the critical region is unattainable due to the high critical temperature (≈10.0 kK). To overcome these limitations, experimental

methods have been developed for dynamic pulsed heating of submillisecond duration [7–11]. For transition metals, there are known data on fast pulsed heating of wires in water and inert gases under pressure, obtained by different authors in [7, 8]. In these studies, the measurements of enthalpy, density, temperature, and electrical resistance were carried out in the temperature range from the melting point T_m to the temperatures of 5.0–7.0 kK. In papers [9–11], which were carried out according to the same technique, the authors managed to experimentally estimate the parameters of the critical points of a number of metals, including gold. Despite significant advances in the experimental technology, the determination of the critical parameters for the most of liquid metals is still not available. For many materials, there are only theoretical estimates within the framework of various models, among which phenomenological methods [12–20] and atomistic modeling methods [21–29] stand out. There are widely used empirical relations that connect the parameters of the critical point with various characteristics of a substance in the liquid and gaseous states. These include the principle of corresponding states based on the similarity laws [12], characteristic lines (for example, the Zeno unit compressibility line) that have gained wide popularity [15, 16, 30], the rectilinear diameter method [2], the critical temperature estimates by extrapolation of the experimentally found dependence of surface tension $\sigma = f(T)$ [17, 18], the estimates of critical parameters based on the relationship of metal vapors with the ionization potential of atoms [13], among these relationships there is also the Kopp–Lang rule [14], relating the critical temperature to the evaporation energy. In [19], a method was proposed for calculating the parameters of the critical points and the binodal of the vapor–liquid phase transition. The model is based on the assumption that cohesion, which determines the main characteristics of metals under the normal conditions, is also responsible for the properties of metals in the vicinity of the critical point. The estimates obtained from semi-empirical equations of state are also widely used [30–33]. In [34], the critical temperatures T_{cr} for 36 liquid metals were estimated from experimental sound velocities using the isochoric thermal pressure coefficient method.

An important tool for the modeling of the properties of substances and of the physical processes that are inaccessible for direct measurement is mathematical modeling based on atomistic models. The atomistic approach is represented by Monte Carlo [20, 27–29] and molecular dynamics [21–26] methods. Within the framework of the Monte Carlo method, the Wang–Landau (EWL) approach is used to determine the critical parameters of metals and nonmetallic substances [27].

Mathematical modeling based on the method of molecular dynamics, over the past two decades, has become a powerful tool for fundamental research of the properties [23, 25–29] and processes [21, 22, 24, 28, 29] in the materials at high temperatures. Molecular dynamics modeling makes it possible to determine the parameters of the phase equilibrium line of the liquid and gas phases and, with their help, to study the near-critical region, where experimental studies are associated with great difficulties. The line of coexistence of liquid and gas phases is of particular interest due to the fact that the boundary curve (binodal) separates homogeneous states of matter from two-phase metastable states. Metastable states of the superheated liquid phase of metals have been relatively little studied [35]. Meanwhile, the solution of many practical problems requires knowledge of the properties of superheated liquid and saturated vapor [36]. In particular, the properties of superheated liquid significantly affect the nature of its boiling, and the properties of supersaturated vapor determine the condensation process [37]. At the critical point, unlike other points of the binodal, the properties of both phases (liquid, vapor) are identical, that is, the critical state is the same limiting physical state for both phases.

Despite the complexity of theoretical and experimental approaches, there is still interest in research in this area.

The purpose of this work is to obtain, using molecular dynamics modeling, the liquid–vapor coexistence curve for gold and to determine the corresponding critical parameters: temperature T_{cr}, density ρ_{cr}, and pressure P_{cr}. For an approximate description of the energy of interaction between particles, the potential of an embedded atom method (EAM) [26] was used. Previously, this potential was used by the authors to determine the thermophysical and mechanical properties of gold in the region of the melting–crystallization phase transition [38].

2. MATHEMATICAL FORMULATION OF THE PROBLEM

The method of molecular dynamics is based on the representation of the object under consideration in the form of a set of particles for which the Newton's equations are written. For each particle, the mass m_i,

the velocity v_i, and the position vector r_i are considered. Thus, a system of $2N$ ordinary differential equations (ODEs) is obtained:

$$\begin{cases} m_i \dfrac{d\mathbf{v}_i}{dt} = \mathbf{F}_i + \mathbf{F}_i^{\text{ext}} \\ \dfrac{d\mathbf{r}_i}{dt} = \mathbf{v}_i \end{cases}, \quad i = 1,\ldots,N, \tag{1}$$

where $\mathbf{F}_i = -\partial U(\mathbf{r}_1 \ldots \mathbf{r}_N)/\partial \mathbf{r}_i$ is the force of the interaction between the particles, $\mathbf{F}_i^{\text{ext}}$ is the force of the interaction with the external fields, $U(\mathbf{r}_1,\ldots,\mathbf{r}_N)$ is the potential energy of the interaction of N particles.

Initial and boundary conditions. At the initial moment of time, the object under consideration is a crystal at a temperature T, the particles are located at the nodes of the crystal lattice. The particle velocities at the initial moment are given as random variables corresponding to the Maxwell distribution at the doubled temperature $2T$.

Periodic conditions are used as boundary conditions. Under periodic boundary conditions along the x axis, it is considered that the particle that has exited through the right boundary is replaced by a particle with the same velocity but entered through the left boundary.

In what follows, the system of ODEs (1) is solved using the Verlet finite-difference scheme in the velocity form [39].

Particles interaction potential. The accuracy of the results of molecular dynamics simulation significantly depends on the particle interaction potential used. To determine the branches of the liquid–vapor coexistence curve and the critical parameters of gold, in this work, we used a potential from the EAM family developed for gold and tested in [26]. The results of the testing of the potential on gold showed its reliability and good agreement with the experimental data.

Calculation of macroscopic quantities. In the course of molecular dynamics modeling of a condensed medium, a local thermodynamic equilibrium is established fairly quickly. Based on this, the main thermodynamic quantities can be determined: pressure (stresses in the crystal) and temperature.

Temperature. As it is known [40], the temperature of the translational degree of freedom $\alpha = x, y, z$ can be obtained by averaging the chaotic component of the kinetic energy over an ensemble of particles with a steady equilibrium distribution:

$$T_\alpha = \frac{1}{k_B N}\left\langle \sum_{i-1}^{N} m_i \left(v_{\alpha i} - \mathbf{v}_{\alpha\text{mid}}\right)^2 \right\rangle_\tau . \tag{2}$$

Here, $\mathbf{v}_{\text{mid}}$ is the translational velocity of the center of mass of the ensemble, k_B is the Boltzmann's constant. The angle brackets $\langle\bullet\rangle_\tau$ imply additional time averaging to reduce fluctuations in the resulting value. Obviously, the averaging interval must be much less than the characteristic time of the processes studied by modeling. The overall temperature is simply defined as the average over the degrees of freedom:

$$T = \left(T_x + T_y + T_z\right)/3. \tag{3}$$

Pressure. The pressure tensor is calculated by averaging over volume and additionally over time [40]:

$$\begin{aligned} P_{\alpha\beta} &= \frac{1}{V_N}\left\langle \sum_{k=1}^{N} m_k (v_{\alpha k} - \mathbf{v}_{\alpha mid})(v_{\beta k} - \mathbf{v}_{\beta mid}) \right\rangle_\tau + \frac{1}{V_N}\left\langle \sum_{k=1}^{N} \mathbf{F}_{\beta k}\alpha_k \right\rangle_\tau \\ &= \frac{1}{V_N}\left\langle \sum_{k=1}^{N} m_k (v_{\alpha k} - \mathbf{v}_{\alpha mid})(v_{\beta k} - \mathbf{v}_{\beta mid}) \right\rangle_\tau - \frac{1}{2V_N}\left\langle \sum_{k=1}^{N}\sum_{j=1,k\neq j}^{N} \mathbf{F}_{\beta kj}\alpha_{kj} \right\rangle_\tau . \end{aligned} \tag{4}$$

Here, V_N is the volume occupied by the ensemble, $\mathbf{F}_k = \sum_{j=0,j\neq k}^{N} \mathbf{F}_{kj}$ is the total force acting on the particle k from the other particles, $\alpha_{kj} = (\alpha_j - \alpha_k)$ is the α-component of the vector $\mathbf{r}_{kj} = (\mathbf{r}_j - \mathbf{r}_k)$. The diagonal tensor elements $P_{\alpha\alpha}$ are the stresses in three spatial directions. In the case of isotropic media (liquids, gases), the pressure can be obtained by simply averaging these components:

$$P = (P_{xx} + P_{yy} + P_{zz})/3. \tag{5}$$

3. COMPUTATIONAL ALGORITHM

The basis of the computational algorithm for determining the critical parameters of gold, temperature T_{cr}, density ρ_{cr}, and pressure P_{cr} is the methods of numerical study of the behavior of a two-phase system: liquid (liquid fraction of Au) and saturated vapor.

The computational domain was chosen in the form of a parallelepiped 64 nm in size along the x axis, in which the sample atoms occupy 32 nm. Gold has a face-centered cubic lattice with a lattice constant $\alpha = 0.406$ nm, which determines the number of particles equal to 63750 in the selected area. Periodic boundary conditions are set along all three axes. The computational domain is partially filled with a model liquid at a temperature known to be lower than the critical one. Particular attention was paid to the choice of the area size. Preliminary calculations were carried out, from which the dimensions of the region were determined in such a way that the liquid–vapor boundary did not disappear as a result of evaporation before the critical temperature was reached. And vice versa, so that the entire area is not prematurely filled with an expanding liquid.

The computational algorithm for obtaining the curve of coexistence of liquid–vapor and critical parameters includes two stages. The first stage is preliminary, it is necessary to prepare the computational domain for performing computational experiments. The second stage is the direct execution of computational experiments. To perform the first and second stages, Berendsen's thermostat and barostat are used [41, 42].

At the second stage, the calculations are organized according to the cyclic principle. Each cycle i ($i = 1, 2, ..., n$) combines heating the sample to the set temperature $T_i = T_{i-1} + \Delta T_{i-1}$, establishing equilibrium between liquid and saturated vapor in the sample at temperature T_i, obtaining the value of saturated vapor pressure $P_{sat}(T_i)$ and density $\rho(T_i)$, refinement of liquid and gold vapor densities to form binodal branches, and selection of the heating parameters – temperature step ΔT_i and heating duration— for the next cycle of operations. The heating step ΔT_i for each subsequent cycle decreased successively in the range (0.40–0.10) kK. The heating time in this case successively increased from 150 ps to 1.5 ns. Heating continued up to the temperature $T \approx 10.0$ kK.

Averaging of MD calculations results. In each sample heating cycle, according to the results of MD simulation, the saturated vapor pressure and density were averaged over time and space. The binodal branches and the temperature dependence of the saturated vapor pressure $P_{sat}(T)$ were formed from the averaged values. Each value of the dependence of the saturated vapor pressure was formed in accordance with (4), (5).

The density values were averaged as follows. Figures 1a and 1b show the spatial distributions of gold density at two temperatures $T = 6.50$ kK (Fig. 1a) and $T = 7.05$ kK (Fig. 1b), averaged over time. It can be seen that on the curve (Fig. 1a) for the temperature $T = 6.55$ kK, two spatial ranges $x_1 \in (-25, -15)$ nm and $x_2 \in (-10, 20)$ nm are clearly distinguished, in which oscillations are around two different density values. In each of these ranges, the density was averaged over space. In the first x_1 range, the average (mid) density $\rho_{mid,1} \approx 1.323$ g/cm^3 was obtained, and in the second x_2 range, $\rho_{mid,2} \approx 6.125$ g/cm^3. Both density values correspond to the same temperature $T = 6.50$ kK.

The first value belongs to the vapor, and the second, to the liquid branch of the binodal at a temperature $T = 6.50$ kK. We get two coexisting phases – vapor and liquid with different densities, while the temperature and pressure of the two phases remain identical.

Figure 1b shows the curve corresponding to the density of gold at $T = 7.05$ kK. On this curve, it is difficult to single out the spatial ranges corresponding to a particular phase. Density fluctuations occur around one average value $\rho_{mid} \approx 3.8$ g/cm^3, that is, the density of liquid and gold vapor is approximately the same in this region, and the temperature is close to critical. The branches of the liquid–vapor phase equilibrium curve obtained by such averaging were plotted on the $\rho - T$ plane. Thus, the initial sections of the branches of the gold phase diagram were obtained up to a temperature of 6.50 kK (see Fig. 4). After reaching this temperature, the value of the critical density was refined as the average density of the vapor and liquid branches of the binodal. This was followed by a restructuring of the computational domain with a new refined density. The calculation of the density and pressure of saturated vapor continued with a rebuilt computational domain at a temperature of $T > 6.50$ kK. Such refinement is necessary to ensure that the computational domain is not filled with liquid or vapor before the critical temperature is reached. Heating is repeated up to a temperature at which density fluctuations do not allow one to separate the density of the liquid and vapor branches. In our calculation, the last temperature value at which the densities of the liquid and vapor branches of the binodal are identified is $T = 6.85$ kK.

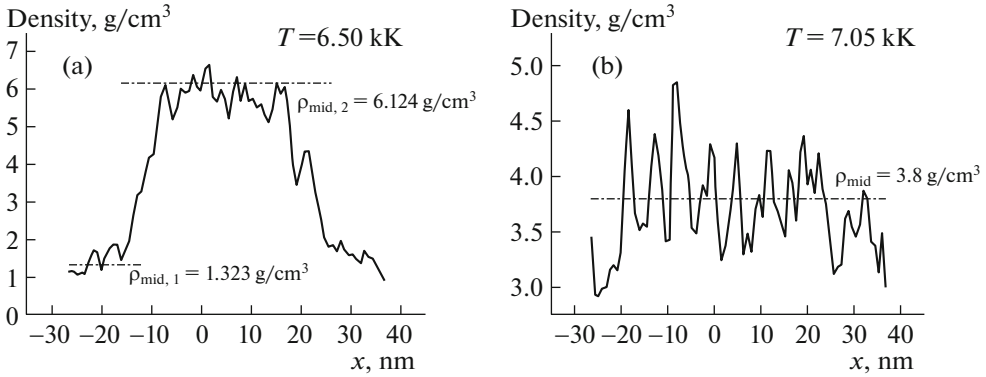

Fig. 1. Spatial distribution of gold density averaged over time: (a) at $T = 6.50$ kK and (b) at $T = 7.05$ kK.

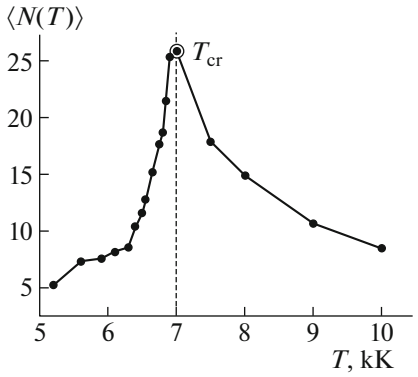

Fig. 2. Cluster size dependence on temperature.

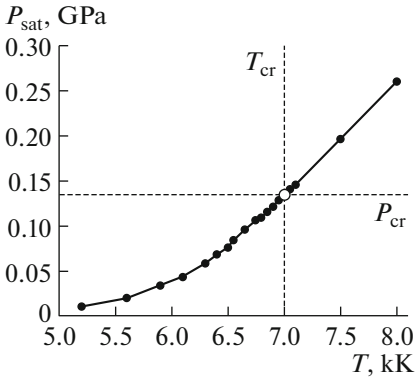

Fig. 3. Temperature dependence of saturated vapor pressure.

4. CRITICAL TEMPERATURE T_{cr} AND CRITICAL PRESSURE P_{cr}

On the phase diagram, the position of the critical point of the liquid–vapor transition is one of the fundamental parameters. To obtain the value of T_{cr}, the method of the maximum size of the averaged cluster on the temperature curve passing through the critical region was used [23, 43].

The essence of the method is as follows. In the subcritical region, with increasing temperature, the density and pressure of saturated vapor increase. In the near-critical region, atomic vapor particles begin

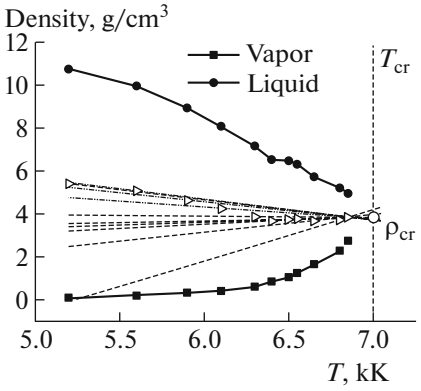

Fig. 4. Binodal of gold.

to combine into clusters, which reach their maximum size just at the critical point. With a further increase in temperature, the density no longer increases. In this case, due to the increase in the kinetic energy of chaotic motion, the fragmentation of clusters into smaller ones begins. Thus, the average cluster size must have a singularity at the critical point. This fact is used in this method to determine the critical temperature. The average number of atomic particles characterizing the sizes of averaged clusters can be estimated by the formula:

$$\langle N(T) \rangle = n(T) k_B T / P_{sat}(T), \tag{6}$$

where $P_{sat}(T)$ is the pressure of the saturated vapor at this temperature T (Fig. 3), $n(T)$ is the concentration of atomic particles in saturated vapor, k_B is the Boltzmann constant.

The temperature dependence of the size of the averaged clusters, shown in Fig. 2, has a pronounced maximum, indicating a change in the mechanism of formation of saturated vapor and further identified with the value of the critical temperature. According to Fig. 2, the value of the critical temperature of gold is $T_{cr} \approx 7.0$ kK. For the first time, this method for determining the critical temperature was proposed in [23, 43] and was called the method of the maximum size of the averaged cluster on the temperature curve passing through the critical region.

The saturated vapor pressure was determined in each heating cycle of the calculation area in accordance with (4) and (5). After averaging over time and space, the saturated vapor pressure curve P_{sat}(T) was plotted (Fig. 3).

Analyzing the dependence of saturated vapor pressure on temperature, one can determine the critical pressure (at a known critical temperature $T_{cr} \approx 7.0$ kK). The specific value of the critical pressure is determined from the intersection of the saturated vapor curve and the vertical straight line corresponding to the critical temperature (Fig. 3) $P_{sat}(T_{cr}) = P_{cr} \approx 0.134$ GPa.

It should be noted that when passing through the critical point, the behavior of the temperature dependence of the saturated vapor $P_{sat}(T)$ changes. A highly imperfect saturated vapor, described by an exponent in the subcritical region, transforms into an ideal one with a linear dependence in the supercritical region (Fig. 3).

5. LIQUID–VAPOR COEXISTENCE CURVE AND CRITICAL DENSITY OF GOLD

The value of the critical density was determined by the empirical rule of the rectilinear diameter [2, 23]

$$\rho_L + \rho_{sat} = 2\rho_{cr} + \lambda(T_{cr} - T), \tag{7}$$

where ρ_L is the density of liquid phase at the temperature T, ρ_{sat} is the density of saturated vapor in equilibrium with liquid at the same temperature. The coefficient λ is different for different materials and is a positive value close to 1.

The name of this rule becomes clear if we take into account that in the coordinates $\rho - T$, the diameter of the curve $\rho(T)$ is a straight line. At $T \approx T_{cr}$, the rectilinear diameter rule has the form

$$\rho_{cr} \approx (\rho_L + \rho_{sat})/2. \tag{8}$$

Figure 4 shows the liquid–vapor coexistence curve obtained from the results of MD simulation at the final stage of determining the value of the critical density ρ_{cr}.

The obtained branches of the binodal are not symmetric; therefore, to refine the critical density, a modification of the rectilinear diameter rule, which has proven itself in [23], is used.

Two points are enough to draw a straight line. As the coordinate of the first point in x, the maximum temperature $T_1 = 6.85$ kK is chosen, which still allows determining the densities of the binodal branches. The ordinate for this point is calculated by formula (8) for the values ρ_L (6.85) and ρ_{sat} (6.85).

As the coordinates of the second point of the rectilinear diameter, one can choose any of the values $T < T_1$ and the average value of the densities of the liquid and vapor branches of the binodal corresponding to this temperature.

In total, 10 variants of the second point D_i ($i = 2, ..., 11$) were calculated and drawn, marked in Fig. 4 by triangular markers. Through the points D_1 and D_i, 10 lines of rectilinear diameter were drawn, indicated in Fig. 4 by dotted lines, and, therefore, 10 density values $\rho_{cr,\,i}$ ($i = 1, ..., 10$) can be obtained at a temperature $T_{cr} \approx 7.0$ kK.

The density value at a known value of $T = T_{cr}$ was determined as the average

$$\rho_{cr} = \sum_i \rho_{cr,i}/10. \tag{9}$$

The obtained value of the critical density is $\rho_{cr} \approx 3.849$ g/cm^3.

Each point on the liquid–vapor curve corresponds to an equilibrium state in which 2 phases can coexist. The branches of the binodal end at one point with coordinates P_{cr}, ρ_{cr}, T_{cr}. As a result of MD simulation, we obtained the coordinates of the critical point $P_{cr} \approx 0.134$ GPa, $\rho_{cr} \approx 3.849$ g/cm^3, $T_{cr} \approx 7.0$ kK, with the help of which the liquid can be continuously converted into a gas along the binodal curve without crossing the phase transition line.

6. COMPARISON OF THE OBTAINED PARAMETERS OF THE CRITICAL POINT OF GOLD WITH THE EXPERIMENTAL ESTIMATES AND THE ESTIMATES OF ALTERNATIVE STUDIES

Table 1 presents the results of the evaluation of the critical parameters of gold from this work, experimental estimates [9–11] (marked with *) and works [12, 17–20, 27, 32, 34]. The values of critical parameters in Table 1 are shown in the order of increasing T_{cr}. Among them, there are estimates obtained: based on the principle of corresponding states [12], by extrapolating the experimentally found dependence of surface tension [17, 18], using the concept of "cohesive energy" [19], using an empirical relation that relates the critical temperature of an element to its solid-state properties [20], as well as the estimates obtained from semi-empirical equations of state [32] and using the isochoric coefficient method [34], as a result of molecular modeling using a many-particle force field, known as the quantum-corrected Sutton–Chen potential [27]. Table 1 also presents the relative deviations of the critical parameters σ obtained in this work from alternative estimates

$$\sigma_{T_{cr}} = \frac{|T_{cr,N} - T_{cr,12}|}{T_{cr,N}}, \quad \sigma_{\rho_{cr}} = \frac{|\rho_{cr,N} - \rho_{cr,12}|}{\rho_{cr,N}}, \quad \sigma_{P_{cr}} = \frac{|P_{cr,N} - P_{cr,12}|}{P_{cr,N}},$$

where $N = 1, ..., 11$ is the ordinal number of the value of critical parameters in Table 1, $T_{cr,\,N}$, $\rho_{cr,\,N}$, $P_{cr,\,N}$ are the critical parameter of other authors, $N = 12$ for the present work.

As it can be seen from Table 1, the critical temperature, density, and pressure obtained in this work are in good agreement with the results of other studies. The results of works [9–11] obtained from the experiment are closest to the obtained value of T_{cr}, the difference is ~3–7%. The values of T_{cr} obtained from alternative calculations [12, 17–20, 32] differ from our calculations by ~15–20%. The greatest difference is observed with the results of works [27, 34]. The critical temperature estimates in these works were obtained using the isochoric coefficient method [34] and from the results of molecular modeling using the quantum-corrected Sutton–Chen potential [27].

The spread of deviations of the values of the critical density ρ_{cr}, as well as the values of T_{cr}, is small and amounts to ~8–36%. The exception is the results of [10] (≈50%). The estimates of the critical pressure are quite different. In addition to [9] (deviation ~3.88%), the obtained value of P_{cr} differs from other works by

Table 1. The values of critical parameters of gold

N	T_{cr}, K	$\sigma_{T_{cr}}$, %	ρ_{cr}, g/cm^3	$\sigma_{\rho_{cr}}$, %	P_{cr}, GPa	$\sigma_{P_{cr}}$, %	Source
1	4048	72.93	–	–	–	–	[34]
2	4286	63.32	5.96	35.42	0.0186	620.43	[27]
3	6250	12	6.1	36.90	1.290	89.61	[19]
4	6520	7.36	4.69	17.93	0.129	3.88	[9]*
5	7217	3.01	3.54	8.73	–	–	[11]*
6	7400 ± 1100	5.41	7.7 ± 1.7	50.01	0.530 ± 0.02	74.72	[10]*
7	7413	5.57	–	–	–	–	[17]
8	8267	15.33	5.0	23.02	0.6265	78.61	[32]
9	8700	19.54	–	–	–	–	[18]
10	8970	21.96	5.68	32.24	0.610	78.03	[12]
11	9087	22.97	–	–	–	–	[20]
12	*7000*	–	*3.849*	–	*0.134*	–	Present work

≈80%. This can be explained by the fact that pressure is the most sensitive characteristic of a substance, reacting to any changes in the system. The results obtained are in good agreement with the experimental results of [9, 11].

7. CONCLUSION

Based on a series of calculations performed using molecular dynamics simulation, a liquid–vapor coexistence curve was obtained and the critical parameters of gold were determined: temperature, density, and pressure using the particle interaction potential from the EAM family [26]. The calculations were carried out using the LAMMPS package [44].

The value of the critical temperature $T_{cr} \approx 7.0$ kK was obtained from the results of MD simulation using the method of the maximum size of the averaged cluster on the temperature curve passing through the critical region [23, 43].

The value of the critical pressure $P_{cr} \approx 0.134$ GPa was obtained from the results of MD simulation from the temperature dependence of the saturated vapor pressure $P_{sat}(T)$.

The determination of the critical value of density $\rho_{cr} \approx 3.849$ g/cm^3 (according to the results of MD simulation) from the binodal curve due to strong density fluctuations near the critical temperature was carried out using the empirical procedure of a rectilinear diameter [2, 23].

Comparison of the modeling results of this work with the results of estimates of the critical parameters of gold obtained from experiments [9–11], as well as those obtained by other researchers using different approaches [12, 17–20, 27, 32, 34], showed a fairly good agreement.

FUNDING

The work was supported by Russian Science Foundation, project no. 18-11-00318.

CONFLICT OF INTEREST

The authors declare that they have no conflicts of interest.

REFERENCES

1. N. Elahi, M. Kamali, and M. H. Baghersad, "Recent biomedical applications of gold nanoparticles: A review," Talanta **184**, 537–556 (2018). https://doi.org/10.1016/j.talanta.2018.02.088
2. M. P. Vukalovich and I. I. Novikov, *Thermodynamics* (Mashinostroenie, Moscow, 1972) [in Russian].

3. R. Winter, C. Pilgrim, F. Hensel, C. Morkel, and W. Gläser, "Structure and dynamics of expanded liquid alkali metals," J. Non-Cryst. Solids **156–158** (Part 1), 9–14 (1993). https://doi.org/10.1016/0022-3093(93)90121-D
4. F. Hensel, E. Marceca, and W. C. Pilgrim, "The metal-non-metal transition in compressed metal vapours," J. Phys.: Condens. Matter **10** (49), 11395–11404 (1998). https://doi.org/10.1088/0953-8984/10/49/026
5. F. Hensel, G. F. Hohl, D. Schaumlöffel, W. C. Pilgrim, and E. U. Franck, "Empirical regularities in the behaviour of the critical constants of fluid alkali metals," Z. Phys. Chem. **214** (6), 823–831 (2000). https://doi.org/10.1524/zpch.2000.214.6.823
6. J. Jüngst, B. Knuth, and F. Hensel, "Observation of singular diameter in the coexistence curves of metals," Phys. Rev. Lett. **55** (20), 2160–2163 (1985). https://doi.org/10.1103/PhysRevLett.55.2160
7. G. R. Gathers, "Dynamic methods for investigating thermophysical properties of matter at very high temperatures and pressures," Rep. Prog. Phys. **49** (4), 341–396 (1986). https://doi.org/10.1088/0034-4885/49/4/001
8. G. Pottlacher (Ed.), *High Temperature Thermophysical Properties of 22 Pure Metals* (Edition Keiper, Graz, 2010).
9. M. M. Martyniuk, "Parameters of the critical point of metals," Zh. Fiz. Khim. **57** (4), 810–821 (1983).
10. K. Boboridis, G. Pottlacher, and H. Jager, "Determination of the critical point of gold," Int. J. Thermophys. **20** (4), 1289–1297 (1999). https://doi.org/10.1023/A:1022687811410
11. W. Schröer and G. Pottlacher, "Estimation of critical data and phase diagrams of pure molten metals," High Temp.—High Press. **43** (2–3), 201–215 (2014).
12. V. E. Fortov, A. N. Dremin, and A. A. Leont'ev, "Evaluation of the parameters of the critical point," High Temp. **13** (5), 984–992 (1975).
13. A. A. Likalter, "On the critical parameters of metals," High Temp. **23** (3), 371–377 (1985).
14. G. Lang, "Critical temperatures and temperature coefficients of the surface tension of liquid metals," Int. J. Mater. Res.: Z. Metallkd. **68** (3), 213–218 (1977). https://doi.org/10.1515/ijmr-1977-680309
15. E. M. Apfelbaum and V. S. Vorob'ev, "The similarity relations set on the basis of symmetrization of the liquid—vapor phase diagram," J. Phys. Chem. B **119** (26), 8419–8424 (2015). doi. https://doi.org/10.1021/acs.jpcb.5b03975
16. E. M. Apfelbaum and V. S. Vorob'ev, "The wide-range method to construct the entire coexistence liquid–gas curve and to determine the critical parameters of metals," J. Phys. Chem. B **119** (35), 11825–11832 (2015). https://doi.org/10.1021/acs.jpcb.5b06336
17. S. Blairs and M. H. Abbasi, "Correlation between surface tension and critical temperatures of liquid metals," J. Colloid Int. Sci. **304** (2), 549–553 (2006). https://doi.org/0.1016/j.jcis.2006.07.072
18. G. Kaptay, "On the order–disorder surface phase transition and critical temperature of pure metals originating from BCC, FCC, and HCP crystal structures," Int. J. Thermophys. **33** (7), 1177–1190 (2012). https://doi.org/10.1007/s10765-012-1270-5
19. A. L. Khomkin and A. S. Shumikhin, "The thermodynamics and transport properties of transition metals in critical point," High Temp. – High Press. **46** (4–5), 367–380 (2017).
20. H. Kanno, "New empirical formula for estimating critical temperature of element from solid properties," J. Inorg. Nucl. Chem. **38** (8), 1573–1575 (1976). https://doi.org/10.1016/0022-1902(76)90036-1
21. V. I. Mazhukin, A. A. Samokhin, M. M. Demin, and A. V. Shapranov, "Explosive boiling of metals upon irradiation by a nanosecond laser pulse," Quantum Electron. **44** (4), 283–285 (2014). https://doi.org/10.1070/QE2014v044n04ABEH015388
22. V. I. Mazhukin, A. A. Samokhin, A. V. Shapranov, and M. M. Demin, "Modeling of thin film explosive boiling—surface evaporation and electron thermal conductivity effect," Mater. Res. Express **2** (1), 016402 (2015). https://doi.org/10.1088/2053-1591/2/1/016402
23. M. M. Demin, O. N. Koroleva, A. V. Shapranov, and A. A. Aleksashkina, "Atomistic modeling of the critical region of copper using a liquid–vapor coexistence curve," Math. Montisnigri **46**, 61–71 (2019). https://doi.org/10.20948/mathmontis-2019-46-6
24. M. V. Shugaev, C.-Y. Shih, E. T. Karim, C. Wu, and L. V. Zhigilei, "Generation of nanocrystalline surface layer in short pulse laser processing of metal targets under conditions of spatial confinement by solid or liquid overlayer," Appl. Surf. Sci. **417**, 54–63 (2017). https://doi.org/10.1016/j.apsusc.2017.02.030
25. D. I. Zhukhovitskii and V. V. Zhakhovsky, "Thermodynamics and the structure of clusters in the dense Au vapor from molecular dynamics simulation," J. Chem. Phys. **152**, 224705 (2020). https://doi.org/10.1063/5.0010156

26. V. V. Zhakhovskii, N. A. Inogamov, Yu. V. Petrov, S. I. Ashitkov, and K. Nishihara, "Molecular dynamics simulation of femtosecond ablation and spallation with different interatomic potentials," Appl. Surf. Sci. **255** (24), 9592–9596 (2009).
https://doi.org/10.1016/j.apsusc.2009.04.082

27. C. Desgranges, L. Widhalm, and J. Delhommelle, "Scaling laws and critical properties for FCC and HCP metals," J. Phys. Chem. B **120** (23), 5255–5261 (2016).
https://doi.org/10.1021/acs.jpcb.6b04121

28. E. M. Apfelbaum and V. S. Vorob'ev, "The Zeno line for Al, Cu, and U," J. Phys. Chem. B **120** (21), 4828–4833 (2016).
https://doi.org/10.1021/acs.jpcb.6b03561

29. J. K. Singh, J. Adhikari, and S. K. Kwak, "Vapor–liquid phase coexistence curves for Morse fluids," Fluid Phase Equilib. **248** (1), 1–6 (2006).
https://doi.org/10.1016/j.fluid.2006.07.010

30. A. A. Likalter, "Critical points of metals of three main groups and selected transition metals," Phys. A: Stat. Mech. Its Appl. **311** (1–2), 137–149 (2002).
https://doi.org/10.1016/S0378-4371(02)00840-3

31. L. V. Al'tshuler, A. V. Bushman, M. V. Zhernokletov, V. N. Zubarev, A. A. Leont'ev, and V. E. Fortov, "Unloading isentropes and the equation of state of metals at high energy densities," Sov. J. Exp. Theor. Phys. **51** (2), 373–383 (1980).

32. D. A. Young and B. J. Alder, "Critical point of metals from the van der Waals model," Phys. Rev. A **3** (1), 364–371 (1971).
https://doi.org/10.1103/PhysRevA.3.364

33. A. A. Likalter, "Equation of state of metallic fluids near the critical point of phase transition," Phys. Rev. B **53** (8), 4386–4392 (1996).
https://doi.org/10.1103/PhysRevB.53.4386

34. S. Blairs and M. H. Abbasi, "Internal pressure approach for the estimation of critical temperatures of liquid metals," Acta Acust. Acust. **79** (1), 64–72 (1993).

35. V. P. Skripov, *Metastable Liquids* (Halsted Press, Wiley, New York, 1974).

36. V. A. Kirillin, V. V. Sychev, and A. E. Sheidlin, *Technical Thermodynamics* (Izd. Dom MEI, Moscow, 2008) [in Russian].

37. F. Hensel, "35 years Liquid Metals conferences: what do we and what do we not yet understand about liquid metals?" J. Non-Cryst. Solids **312–314**, 1–7 (2002).
https://doi.org/10.1016/S0022-3093(02)01640-X

38. V. I. Mazhukin, O. N. Koroleva, A. V. Shapranov, M. M. Demin, and A. A. Aleksashkina, "Determination of thermal properties of gold in the region of melting–crystallization phase transition: Molecular dynamics approach," Math. Models Comput. Simul. **14** (4), 662–676 (2022).
https://doi.org/10.1134/S2070048222040068

39. L. Verlet, "Computer "experiments" on classical fluids. I. Thermodynamical properties of Lennard-Jones molecules," Phys. Rev. **159** (1), 98–103 (1967).
https://doi.org/10.1103/PhysRev.159.98

40. V. I. Mazhukin and A. V. Shapranov, "Molecular-dynamic modeling of processes of heating and melting of metals. Part I. Model and computational algorithm," KIAM Preprint No. 31 (Keldysh Inst. Appl. Math. RAS, Moscow, 2012) [in Russian].

41. H. J. C. Berendsen, J. P. M. Postma, W. F. van Gunsteren, A. DiNola, and J. R. Haak, "Molecular dynamics with coupling to an external bath," J. Chem. Phys. **81** (8), 3684–3690 (1984).
https://doi.org/10.1063/1.448118

42. M. P. Allen and D. J. Tildesley, *Computer Simulation of Liquids* (Clarendon Press, Oxford, 2002).

43. V. I. Mazhukin, A. V. Shapranov, O. N. Koroleva, and A. V. Rudenko, "Molecular dynamics simulation of critical point parameters for silicon," Math. Montisnigri **31**, 56–76 (2014).

44. S. Plimpton, "Fast parallel algorithms for short-range molecular dynamics," J. Comput. Phys. **117** (1), 1–19 (1995).
https://doi.org/10.1006/jcph.1995.1039